Sensors and Materials, Vol. 19, No. 1 (2007) 035–056
MYU Tokyo

S & M 0665

Designing and Fabricating Electromagnetically Actuated Microvalves for MEMS Applications

J. Sutanto[**], R. Luharuka[***], P. J. Hesketh[*] and Y. H. Berthelot

The George W. Woodruff School of Mechanical Engineering,
Georgia Institute of Technology, Atlanta, GA 30332-0405

(Received May 25, 2006; accepted: February 2, 2007)

Key words: microvalve, electroplating

This paper reviews our work on microfabricated miniature electromagnetic microvalves. Three different designs are presented: on/off, mechanically bistable, and rotational microvalves. This paper concentrates in the design, modeling/simulation, and the fabrication of different types of electromagnetic microvalves. The challenges in the fabrication of permanent magnets directly on the valve's membrane structure to produce bistable techniques are also presented.

1. Introduction

Microvalves are key components in miniature fluidic systems. The use of MEMS actuation for active control of microvalves to direct fluid routing is an important application where the proper scaling of the actuator helps improve the fluid control. In particular, it also decreases the dead volume and power consumption of the valve, and increases the speed and stroke of the actuator. Given the diverse range or applications, the design requirements can vary a great deal. The desired specification, including fluid flow parameters, in addition to the compatibility and cost of the manufacturing process should also be carefully considered. Applications range from miniature gas chromatography systems to biosensing and analysis systems to fuel cells, precision manufacturing processes to medical devices, such as drug delivery. The requirements for a specific application have a significant impact on the appropriate design and this is the topic we wish to consider in this paper.

*Corresponding author, e-mail address: peter.hesketh@me.gatech.edu
**now at Intel Corporation, Chandler, AZ 85226
***now at Schlumberger, Sugar Land, TX 77478

A couple of important questions to consider are should the valve be integrated with the MEMS device or the with the IC or CMOS circuit or should it be assembled after the manufacturing process is complete. The energy consumption of the electromagnetic microvalve can be reduced significantly by using a bistable technique. Application of power for a short duration in the order of milliseconds is all that is needed to latch or unlatch the valve. Key attributes include the integration of magnetic materials for the large stroke electromagnetic actuation principle. For this case, both hard and soft magnetic materials can be electroplated into a photoresist mold to define the desired structures.

The development of microactuators has been a significant topic of research in MEMS technology which frequently required integration of non-IC standard materials. In Table 1 several different choices of microactuation for microvalve are summarized. The simplest microactuators consist of a beam or a membrane as the moving part and an external force which can be generated by several methods. These include piezoelectric,[1,2] electrostatic,[3–11] electromagnetic,[12–15] thermal bimorph,[16–19] thermo-pneumatic,[20–22] shape memory alloy,[23–25] and hydrogel.[26–28] The electromagnetic method has several advantages compared to other methods of actuation: low/efficient power consumption[29–31] and ability to produce large membrane displacements.[32] Indeed electromagnetic actuator have been utilized for various applications, including for instance RF switches,[29,30] optical switches, magnetic sensors,[33] microvalves,[12,15,34] and combined optical and magnetic sensors.[33] Typically piezoelectric and electrostatic actuation requires high voltage. Meanwhile thermal bimorph actuators require large temperature changes, which may locally boil the working fluid or degrade the protein in a biological application. Thermo-pneumatic actuators benefit from the combination of thermal and pneumatic techniques to provide large forces but typically involve high temperature operation or an external supply of pneumatic drive. Actuation based upon hydrogels is typically slow because their operation depends upon the change of the external environment and diffusion into the hydrogel. Hence, our work has focused on integration of electromagnetic actuation because it produces a large displacement with low operating voltage and low energy consumption when operated in a latching mode.

In this paper a review of our work related to three types of microvalve are presented. The studies are discussed based upon the works we have directly been involved with in developing microfabricated electromagnetic microvalves. On-off, latching, and rotational valve designs are discussed. Most of the microvalves fabricated by surface micromachining involve the use of at least two Si wafers, which are then clamped together by bonding mechanism. To achieve a monolithic integration of the microvalve with the IC circuits, the microvalve has to be fabricated on a single Si (silicon) wafer. Another requirement is that the microvalve fabrication then must be CMOS compatible with the maximum fabrication temperature of 400°C.[43] Low power consumption and low voltage (< 5V) are important requirements for the microvalve, particularly when the lab-on-a-chip is used in mobile installations. There is a more complete review in the book by Nguyen and Wereley on microfluidics[44] a recent review paper on microvalves[45] and book chapter on microvalves.[46] Miniature electromechanical valves are also commercially available (Lee Valve Company, www.theleeco.com).

Table 1
Microvalves for different kinds of actuator, showing the specifications for controlling the flow of DI water.

Type	*Act*	*D* μm	Size mm^2	*V* V	*I* A	*P* W	*HP* W	*S*/*RT* ms	*FR* μL/min	*LR* μL/min	*MFP* kPa	*#FS*
Cantilever[12]	EM	150	100	1–2	0.29	0.29 –0.58	No	30 –80	0–420	—	2	2
Membrane[35]	EM	< 50	81	< 2.5	0.01–0.065	< 0.16	< 0.16	—	—	—	6.8	4
Silicon rubber seat[36]	P	—	35.7	59 kPa	(N/A)	(NA)	59 kPa	1000	0–1000	0.1	108	4
PDMS membrane[37]	P	—	—	60 kPa	—	—	60 kPa	—	0–20	—	20	3
Micro heater[38]	TP	—	38.5	—	—	0.158	0.158	—	10,260	—	18	3
Pinch valve (normally close)[39]	SM	—	—	—	—	0.398	0.398	—	16,800	—	204	N/A
Membrane /diaphragm[40]	PZT and EST	13	81	145 –148	—	—	—	10 –40	–40 –80	—	10	3
Membrane[26]	H	185	—	2–11 (pH)	N/A	N/A	N/A	mins	10	—	292	5
Membrane[41]	EM	12	0.79	1.4–1.9	0.27 –0.6	0.3–1.1	0.3–1.1	—	1	0.03	15	1
Membrane[42]	EM	30	2	3–3.5	0.38 –0.43	1.2 –1.6	No	10	10–50	0.16 –0.8	57	1

Where: *Act* = actuation type; *D* = actuator displacement; *V* = operational voltage; *I* = operational current; *W* = operational power; *HP* = holding power to keep valve closed/open; *S*/*RT* = switching/response time; *FR* = flow rate; *LR* = leaking rate; *MFP* = maximum fluid pressure; *#FS* = number of fabricated substance.
EM: electro magnetic; P = pneumatic; TP = thermopneumatic; SM = shape memory; PZT = piezoelectric; EST = electrostatic; H = hydrogel.

2. Design

The design process of an electromagnetically actuated microvalve can be divided into three different domains: fluidic circuit design, structural components design, and electromagnetic actuator design. Each of these three design areas have been considered separately to highlight their key features. The design process often starts with laying down specifications for the target microvalve such as fluid type, flow conditions (pressure, flow rate, and temperature), permissible leak rate, power rating, overall size, and desired switching time. It is then followed by a concept generation and selection process in which the different types of valve architectures are compared and the best concept is selected,

which closely matches to the target specifications. In the following subsections, issues related to the three different design areas are discussed.

2.1 *Fluidic circuit design*

Fluid flow condition is the most important criterion that is considered for the design of any microvalve. The flow demand in a microfluidic system greatly determines the electromagnetically actuated (EM) microvalve architecture. For applications that require low to medium flow rates (up to few sccm of gas flow), microvalves design with a suspended diaphragm over an inlet hole are more suitable. Our group developed a diaphragm-type, EM *on/off* microvalve to switch methanol flow of 1 µlpm[47] (see Fig. 1(a)). The overall size of the valve, with an integrated current carrying coil for electromagnetic actuation of the suspended diaphragm, was only 1.1 mm in diameter. However, at high flow rates, these microvalve experienced high pressure drop, thus requiring much higher electromagnetic force to switch to an *off* state. Therefore, other microvalve architectures must be considered, which can address to higher flow demands. A cantilever-type EM microvalve was developed by Capanu *et al.*[12] to allow flow rates of up to 30 µlpm of water. The cantilever design of the diaphragm provided larger gap size in the open state, while keeping the leak rate acceptable in the closed state. The squeeze film damping in this design is also expected to be lower due to the angular motion of the cantilever about its pivot point as seen in Fig. 1(b). Another class of microvalves that can be used for fluid flow modulation in a system with high flow rate demand is a gate valve design. Gate valve design overcomes the limitations of the diaphragm-type microvalves such as restricted fluid flow path in the gap region under open condition and insufficient EM actuation force to close the microvalve under high flow rates. The first gate microvalve was reported by Walters *et al.*,[48] which used thermal actuation and achieved gas flow of 5000 sccm at 10 psig. A few different designs of gate microvalves have been reported in the literature,[49–52] which operate in either gas or liquid and have used thermal based actuation method. Also, high flow rate valves have also been demonstrated by Henning *et al.*[53] which incorporate a thermopneumatically actuated diaphragm and is suitable for gas flow control in semiconductor processing applications. An EM gate microvalve as proposed by Luharuka *et al.*[54] can overcome some of the limitations posed by the previous designs such as slow switching, large size, and/or high energy consumption. The gate in this design rotates in-plane between its bistable positions when actuated by an inductor, thus opening and closing the inlet/outlet ports on the substrate (see Fig. 1(c)).

In most microvalve architectures, typical fluid flow path is quite similar. In the open state, fluid enters the valve through an inlet hole and then flows through a restricted gap region between the diaphragm and valve seat (except in gate valve) before exiting through an outlet hole. Fluidic circuit design involves the designing of the inlet and outlet fluidic ports, gap sizing between the diaphragm and valve seat, and the diaphragm size. These parameters directly influence the flow characteristics in the microvalve and must be carefully investigated to match the design specifications. For example, the ratio of gap size and inlet hydraulic diameter delineates the flow into three regimes: seat (or gap) controlled flow; transition flow; and orifice controlled flow.[55] In the seat controlled flow, the valve seat design as demonstrated by Henning[56] becomes a critical parameter in determining the

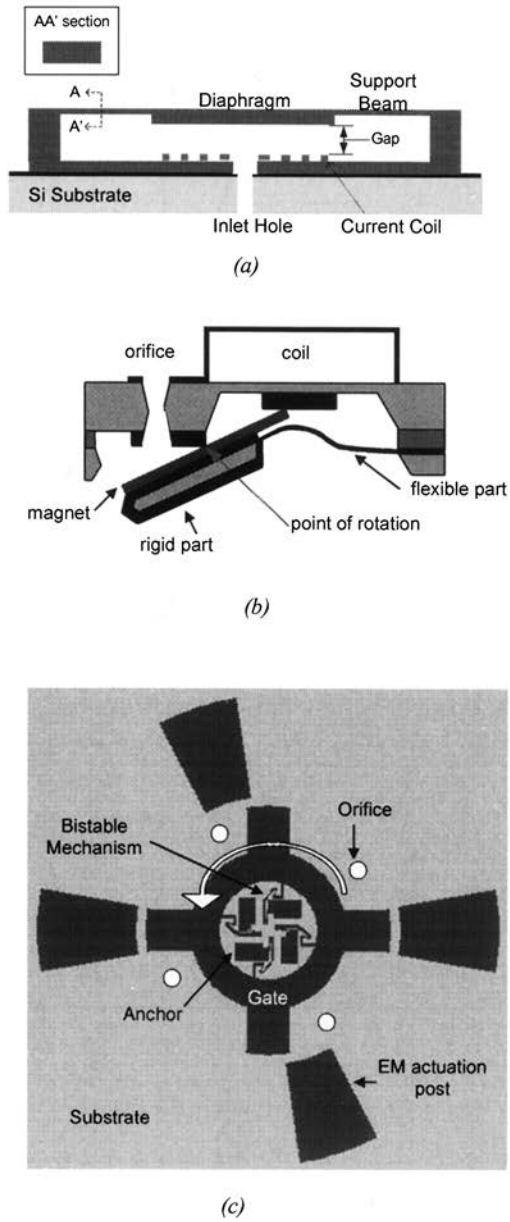

Fig. 1. Three different architectures of electromagnetically actuated microvalves; (a) Diaphragm-type microvalve,[47] (b) Cantilever-type microvalve,[57] and (c) gate microvalve.[58]

flow ratings. Operating fluid has significant influence on the sizing of the fluidic channels. Liquid operated microvalves experience high viscous forces as compared to gases. However, the leakage rate is significantly high in gases, thus requires a larger valve seat area.

Leakage in microvalve is influenced by the valve seat material and its design, operating pressure drop, closing force and roughness at the sealing interface.[53]

2.2 *Structural components design*

The microvalve diaphragm is suspended over the valve seat by a micro-mechanism which is designed to perform kinetic motion between the two positions (*open* (*on*)*/close* (*off*) states) when subjected to an electromagnetic actuation. In a diaphragm-type valve, a set of compliant beams supports the diaphragm and allows its out-of-the-plane linear motion that enables the diaphragm to open and close the inlet orifice. The diaphragm and the support beams are made of soft magnetic material such as a NiFe alloy for electromagnetic actuation by the current carrying coil. The cantilever-type bistable mechanism in Capanu *et al.*[12] performs an out-of-the-plane rotational motion about its pivot point under the influence of the magnetic forces generated by the electrical current flowing in the coil. The gate valve micromechanism performs in-plane rotational motion to switch between *on* and *off* states. Bistability is an important attribute of compliant mechanisms used to control the diaphragm. It is defined as the property of the mechanism, by virtue of which, it has two stable states of equilibrium (a stable equilibrium state is defined at the configuration in which the energy stored in the mechanism is a local minimum). The power requirement during the switching operation in an EM microvalve can go up to a few hundred milliwatts. Providing such high power continuously to maintain the switched state of a microvalve is not practical in portable applications. In addition, this may result in the overheating of the coil due to Joule heating effect. Therefore, bistable design of the compliant mechanism is often necessary in this category of microvalves. It obviates the need for an actuating force to maintain the deflected position of the diaphragm.

2.3 *Electromagnetic actuator design*

Two principle methods of electromagnetic actuation has been used in microvalves, (a) magnetic actuation,[59] and (b) Lorenz force actuation.[60] All the three designs presented in this paper the based on the magnetic actuation. Magnetic force is exerted by a current carrying coil on a diaphragm made of a soft magnetic material, which is located across a small gap. Together they form a path of least reluctance through the air gap as shown in case of the diaphragm-type microvalve in Fig. 2. Most of the microvalve structure is fabricated using a soft magnetic material (except for the current carrying coil) that gets easily magnetized under the influence of a magnetic field and demagnetizes in the absence of one. NiFe alloys such as Permalloy ($Ni_{80}Fe_{20}$), and Orthonol ($Ni_{50}Fe_{50}$) have commonly been used in a wide variety of applications for electromagnetic actuation. Though NiFe alloys have excellent magnetic properties at low temperatures, they are not suitable for higher temperature operations (greater than 150°C). Iron-Cobalt alloys (Permendur) have high Curie temperature ($T_c \approx 900$°C), which makes them a candidate material for high temperature applications. Besides, these alloys have very high saturation induction (B_s = 2.4 T).[61] Properties are listed in Table 2.

The magnetic force is often estimated using a reluctance model of the magnetic path. As a case study, a simplified reluctance model of diaphragm-type microvalve is considered here. The equivalent magnetic circuit shown in Fig. 2 consists of the magnetomotive force

Table 2
Relevant properties of soft magnetic materials.

Magnetic properties	Permalloy (Ni_{80}/Fe_{20})	Orthonol (Ni_{50}/Fe_{50})	Supermendur ($Co_{49}/Fe_{49}/V_2$)
Saturation induction (T)	1.0	1.41	2.4
Operating temperature (°C)	150	150	580
Yield strength (MPa)	200	—	460
Coercivity (Oe)	0.65	1.3	2
Intrinsic stress (MPa)	Up to 130 MPa	Higher than permalloy	Up to 140 MPa
corrosion	low	medium	high

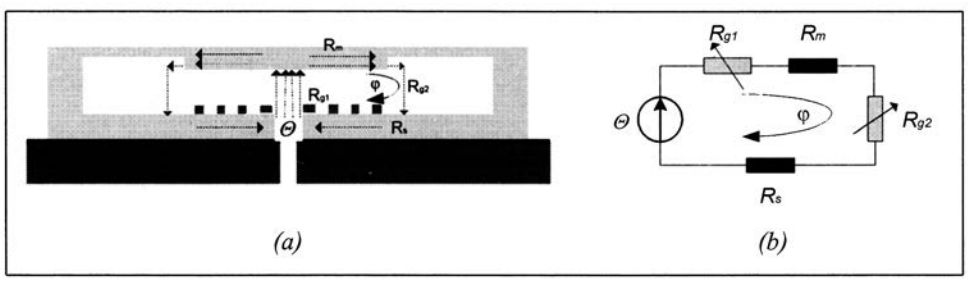

Fig. 2. (a) Magnetic flux path generated by the current carrying coil; (b) Equivalent magnetic circuit of the microvalve.

(Θ) produced by the coil current (I), the reluctance R_{g1} of the air gap between the diaphragm and the coil, the reluctance R_m of the Ni/Fe diaphragm, the reluctance R_{g2} of the return path between the diaphragm and the substrate, and the reluctance of Ni/Fe layer on the Si substrate (R_s). The magnetic flux in the circuit for the unsaturated magnetic circuit is then given by

$$\phi = \frac{\Theta}{(R_{g1} + R_m + R_{g2} + R_s)} \qquad (1)$$

$$\Theta = NI$$

where ϕ is the total magnetic flux entering the membrane, and N is the number of coil turns.

The reluctances of the magnetic path are calculated by the general equation

$$R = \frac{L}{\mu_0 \mu_r A} \qquad (2)$$

where, L is the length of the path in meters, μ_o is the permeability of air, μ_r is the relative

permeability, and A is the area normal to the flux.

The magnetic force exerted on the diaphragm is then given by

$$P = -\frac{\partial \phi}{\partial g} \tag{4}$$

The electromagnetic force on the diaphragm is inversely proportional to the square gap distance (approximately). The magnetic force gets stronger as the diaphragm moves towards the coil during the valve closing. However, this approach only provides a rough estimate for the magnetic force on the diaphragm as a function of gap size and magnetic fluxes. It does not account for various magnetic losses, saturation, and leakage in the circuit. A more rigorous modeling using finite element analysis is necessary to accurately estimate the magnetic forces generated by the current coil in such complex geometry.

2.4 *Integration and design optimization issues*

Integration of the fluidic ports, diaphragm structure, and electromagnetic actuator is a design optimization problem that requires a system level design approach. Integration involves consideration of overall performance of the microvalve such as size, leak rate in *off* state, fatigue life cycle of the valve, valve closing time, energy consumption, and packaging. Though the above three subsections discuss the design issues related to different domains separately, most of the critical design parameters directly or indirectly influence performance in all the three domains. For example, gap size is one such critical parameter which influences fluid pressure drop in the gap region, magnetic force on the diaphragm, and stress in the micromechanism. Though small gap size is preferred for high magnetic force on the diaphragm, it adversely affects the pressure drop in the microvalve. The maximum flux density in the gap is limited by magnetic saturation of the soft magnetic material. Therefore, all these different design parameters should be optimized with respect to performance functions generated from all the three domains.

3. Modeling and Simulation

Finite element methods provide a powerful tool to model a multiphysics system such as a microvalve. In principle, all the three physical domains-fluidic, structural, and electromagnetic can be modeled together to simulate the performance of a microvalve design under different operating conditions. Though these models can provide a more accurate analysis of the microvalve operation than various analytical models discussed, model three-dimensional geometry is complicated and may require large resources due to low aspect ratio of the valve features. It may be advantageous to use a hybrid approach as suggested here to reduce model size and complication without compromising accuracy.

3.1 *Case study of diaphragm-type EM microvalve*

The modeling approach presented here uses a combination of analytical model and multiphysics finite element modeling to predict the valve operation under open condition.

The results are then compared to validate the modeling approach. The details of modeling can be found in the published work by the authors.[46,62] The model uses an analytical model for the magnetic force acting on the diaphragm in a fluid-structural finite element model to simulate the valve operation in open air condition. The magnetic force model is developed using the reluctance method similar to the illustration presented in Fig. 2. This model may be verified and improved using a separate finite element model to simulate the magnetic force on the diaphragm. Figure 3 shows the magnetic flux density in the microvalve structure (Orthonol) at excitation current of 0.7 A in the 8-turns coil. There could be a considerable deviation from the magnetic force predicted by the reluctance model near the saturation limit of material.

The valve closing dynamics and estimation of the closing time, which involves interaction of electromagnetic force, structural spring force and squeeze film damping on the diaphragm can be modeled using a fluid-structural interaction (FSI) model as shown in Fig. 4. The model uses the arbitrary Lagrangian Eulerian (ALE) technique that has been used in the literature to model such highly non-linear, large displacement, fluid-structure interactions.[63] The model is solved for open-air boundary conditions to simulate the test conditions. Since the valve is symmetric about the two vertical planes, only a quarter model with symmetric boundary conditions is built. Inlet and outlet ports are modeled away from the membrane region to prevent influences of the flow boundary constraints on the membrane dynamics. The fluid side of the model is meshed using FLUID142 elements (an eight-noded 3D fluid-thermal element) and the solid side, the membrane and support legs, is meshed using SOLID45 elements (eight-noded element having three degrees of freedom at each node: translations in the nodal x, y and z directions). Since the velocity gradient of the fluid near the wall is high, the fluid volume in the model is map-meshed with a higher density of elements near the walls. The common surface nodes on the fluid

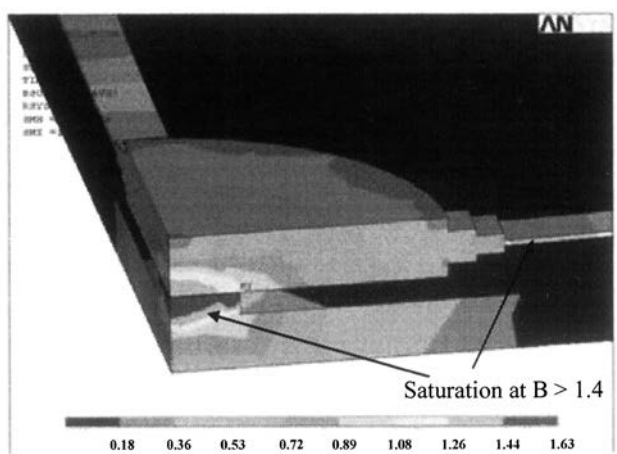

Fig. 3. The magnetic results of the 3D model developed in ANSYS showing the magnetic flux density (B, unit: T) at I = 0.7A.[62]

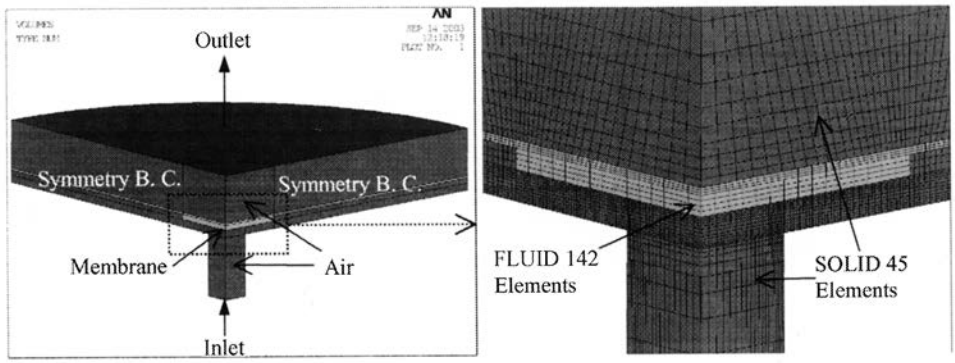

Fig. 4. Three-dimension finite element model of the microvalve in ANSYS 7.0.[46]

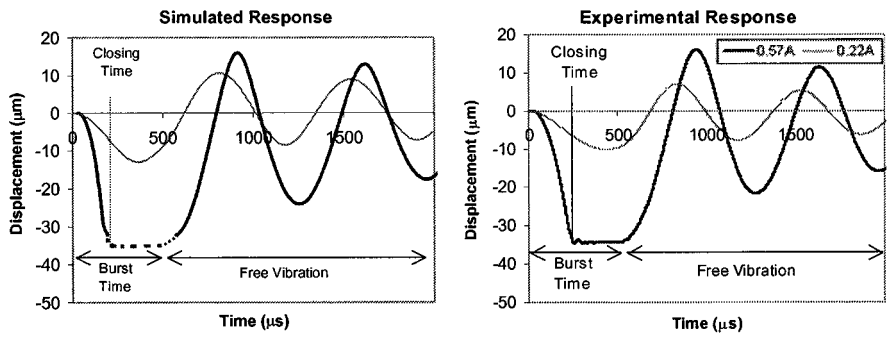

Fig. 5. Comparison of simulated response of the microvalve diaphragm with the test results measured using a laser vibrometer under open air conditions.[46]

and solid sides are flagged for fluid-structure interactions (FSI) such that, during the fluid-structure weak coupling analysis, load transfer takes place between the fluid and structural interfacing nodes. The viscous forces and the pressure of the fluid are transferred as a load to the structural nodes, which takes into account the squeeze film damping and pressure gradient effects of the gas on the diaphragm. The ALE formulation is set for the fluid side to allow for mesh motion and remeshing as the diaphragm moves. To account for the compressibility in the air medium, the bulk modulus of the fluid is set to that of air. The bulk modulus is represented as $\partial p/\partial \rho$ where p is the pressure and ρ is the density. For an ideal gas, it is given by RT where R is the ideal gas constant, and T is the temperature.

The simulated membrane dynamics of the microvalve under open-air condition is compared with the test results obtained using a laser vibrometer (Fig. 5). In general, the simulated results agree well with the test results. In both the simulation and the experimental results, the valve membrane demonstrates an under-damped vibration response when actuated. The valve closes across the gap size of 34 μm during the actuation (burst) time at 0.57A current. However, at lower coil current (0.22A), the membrane undergoes forced and free vibration.

4. Fabrication of On/Off and Bistable Microvalves

On-off, latching bistable and bidirectional microvalves have been developed based upon low temperature fabrication processes that do not exceed 250°C. This allows the valve fabrication to be carried out on a silicon substrate which has already undergone CMOS circuit fabrication processing. Full details are given in the publications for the on/off valve,[41] latching bistable valve,[64] and bidirectional actuators.[65]

Figure 6 shows SEM pictures of the on/off microvalves that have been fabricated. The overall size of the microvalve is 1,100 μm; this includes a membrane with centered dome of 500 μm and a microcoil underneath with the width (*W*) of f 8 μm and height (*H*) of 10 μm. There is a gap of 12 μm between the centered soft magnetic dome and the microcoil surface.

As shown in Fig. 6, the microvalve structure has two electrical connections for the microcoil, the positive and the negative connections. The negative connection is basically connected to the base of the microvalve with SiO_2 as the insulation layer. In the first generation of microvalve, several fabrication issues have been experienced, including the difficulty of etching the microcoil seed layer. As shown in Fig. 6, the membrane has corrugated holes to facilitate the flow of etchant for etching the seed layer in between microcoil turns.

Electroplating has been selected to build the microvalve structure. The process is relatively simple and inexpensive. The deposition rate is much faster than other metal deposition process such as DC Sputter, RF Sputter, and Chemical Vapor Deposition. There are four different electroplating solutions that have been used to build the microvalve structure: Permalloy (Ni_{80}, Fe_{20}), Orthonol (Ni_{50}, Fe_{50}), Au (gold), and hard magnetic material, such as CoNiMnP and CoPt alloys. The hard magnetic material is polled after electroplating to define the permanent magnetic layer.

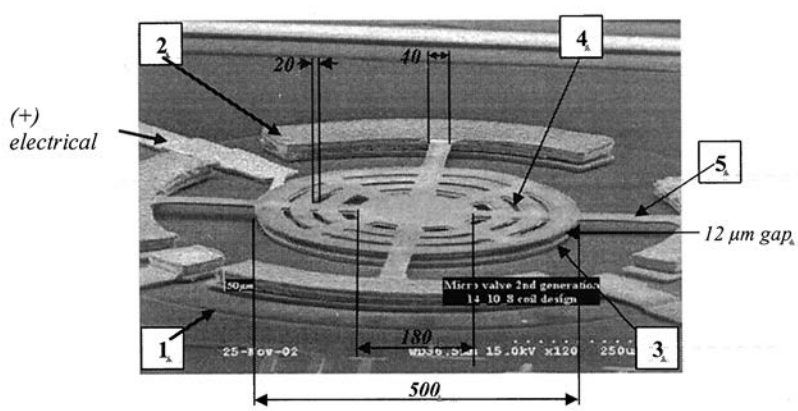

Fig. 6. SEM micrograph of the on/off microvalve (*All dimensions are in μm*); Where: 1 = microvalve's base, 2 = circular support, 3 = Au microcoil, 10 μm thick, 4 = Centered membrane with corrugated holes, and 5 = membrane supported legs, 3 μm thick.

4.1 *Permalloy and Orthonol electroplating*

Permalloy and Orthonol are soft magnetic materials. Permalloy is used to build the circular supports (label no. 2) and centered soft magnetic membrane (label no. 4) as shown in Fig. 6. Orthonol is used to build the base of the microvalve (label no. 1) and the membrane supported legs (label no. 5) as shown in Fig. 6. The recipe for the electrolytes is shown in Table 3.

In the electroplating process Ni foil is used as an anode to maintain a constant metal (Ni) ion composition in the bath. The pH level of the bath is maintained at 2–3. The temperature of the bath is maintained at room temperature 22°C for Permalloy and 50°C for Orthonol. The electroplating bath composition is adapted from ref. 66 and modified for our purpose as described in Table 3. The electroplating was done using pulsed current. The parameters of pulsed electroplating include: current density (J), duty ratio (DR), and bias, which are determined by the following eq. 4:

$$J = \frac{I_H}{A_{plating}}; \quad DR = \frac{t_{on}}{t_{period}}.100\%; \quad bias = \frac{I_L}{I_H}.100\% \tag{4}$$

where: $A_{plating}$ is the total electroplated area, I_H is the maximum current of pulsed plating, t_{on} is the time duration for I_H, and t_{period} is the total time for both I_H and I_L.

A Solartron SI 1287 electrochemical interface is used to control the pulsed current flowing through the electrodeposition cell. The 1.4 lt. electrolyte with the recipe shown in Table 3 is placed into 1.5 lt. beaker. A continuous magnetic stirrer is provided to ensure that a uniform bath composition is attained. The electroplating was done at the J = 30 mA/cm^2, DR = 40%, and Bias = –10%. The deposition rate is varied with the surface condition; it is approximately 0.15–0.16 μm/min for Permalloy and 0.18–0.19 μm/min for Orthonol.

Prior to electrodeposition, a seed layer must be deposited on the wafer. The seed layer consists of a 300 Å layer of titanium (Ti) and a 3000 Å layer of copper (Cu), they are deposited with the use of DC sputtering, by CVC Products Inc., model: CVC-601. The metal composition of the Permalloy and Orthonol are measured by using EDX. The machine is a Hitachi S800 FEG scanning electron microscope (SEM). For Permalloy it shows that the composition of the Ni and Fe are much in agreement with the reported literatures,[9] which are 80 and 20% respectively. Figure 7 shows that the metal composi-

Table 3
Chemical composition of electroplating bath for Permalloy.

Chemical name	Chemical compound	Permalloy (gr/L)	Orthonol (gr/L)
Nickel sulfate hexahydrate	$NiSO_4.6H_2O$	200	168
Ferrous sulfate heptahydrate	$FeSO_4.7H_2O$	8	81
Nickel chloride hexahydrate	$NiCl_2.6H_2O$	5	135
Boric acid	H_3BO_3	25	50
Saccharine		3	3
Ascorbic acid		1	1

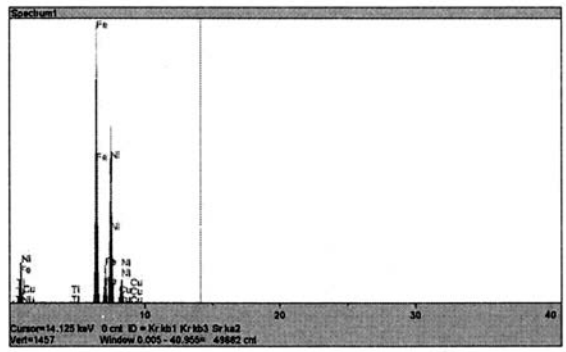

Fig. 7. Metal composition of Orthonol deposited on top of silicon wafer with 300 Å of Ti and 3000 Å of Cu seed layers. It shows the compositions of: 48% Ni, 51% Fe, and 1% of Ti and Cu.

tion of the Orthonol is measured by EDX. The compositions are 48% Ni, 51% Fe, and about 1% of impurities: Ti and Cu.

4.2 *Gold electroplating*

Gold is used as the material for the microcoil (label no. 3) as shown in Fig. 6. The gold is deposited by electroplating in a non phosphate-gold cyanide solution produced by Technic Inc. (Cranston, Rhode Island). This solution is ready to use, the part no: 434 HS solution with 0.25 tr.oz of gold/qt. solution. The gold plating solution is maintained at room temperature with the pH level: 5–7. Platinized aluminum is used as the anode. The gold electroplating is done by direct current at the J = 2–3 mA/cm^2. The deposition rate is about 0.15–0.17 μm/min. The metal composition of the electroplated gold is measured by EDX and the result is shown in Fig. 8 below. The compositions are: 95% Au, 3% Pt, and 2% impurities of Ti and Cu.

4.3 *Co-Pt electroplating*

Co-Pt is one of the alloys that are selected to fabricate the permanent magnet for the bistable microvalve. The magnet is placed underneath the centered soft magnetic dome (label no 4) as shown in Fig. 6. The recipe of the electrolyte is adapted from ref. 67 and modified for our purpose as shown in Table 4 below. Co foil is used as the anode to maintain the constant metal ion composition in the bath. The solution is very corrosive, so extra handling is required during the fabrication process. The pH level of the solution is maintained around 8.

The 1.4 lt. electrolyte with the recipe shown in Table 4 is placed into a 1.5 lt. beaker. A continuous magnetic stirrer is provided to ensure that a uniform bath composition is attained. There are several difficulties encountered during the deposition of thick film Co-Pt permanent magnet, especially when thickness is greater than 5 μm. The two major difficulties are: bubble production and surface cracking. H_2 gas bubble is the non-preventable product from electroplating process. The gas bubbles produced a rough/non-

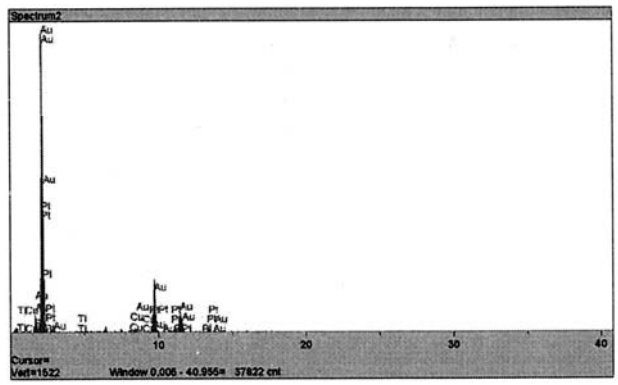

Fig. 8. The metal composition of the gold (Au) deposited on top of silicon wafer with 300 Å of Ti and 3000 Å of Cu seed layers. It shows the compositions of: 95% Au, 3% Pt, and 2% of Ti and Cu.

Table 4
Chemical composition of electroplating bath for Co-Pt permanent magnet.

Chemical name	Chemical compound	gr/L
Diammine platinum (II) nitrate	$Pt(NO_2)_2(NH_3)_2$	3.21
Cobalt (II) sulfamate	$Co(NH_2SO_3)_2$	25.11
Ammonium citrate	$(NH_4)_2C_6H_6O_7$	22.62
Glycine	NH_2CH_2COOH	7.51
Saccharin		2
Sodium hypophosphite monohydrate	$NaH_2PO_2.H_2O$	10.6

uniform plating surface, bubbling, and cracking of the photoresist. The bubble production became more pronounced for thicker deposition, $t_M > 10$ μm. In order to minimize the bubble production, the wafer was taken out from the electrolyte bath every 10 min to remove the bubbles to the air.

Co-Pt deposition produces a tension stress, with a value that depends on the Co composition, for example, for 80% Co, the stress is about 250 MPa.[31] In order to reduce the stress from Co-Pt deposition to 100 MPa, 2 gr/L of saccharin is added to the electrolyte and the electrolyte temperature is increased from room temperature to 40–50°C. The increase of the electrolyte temperature may soften and taper the sidewall of AZ4620 photoresist mold.

Very serious cracking and large grain size ($D_h > 10$ μm) were experienced for the Co-Pt deposition at room temperature, 20–25°C. Figure 9(a) shows the SEM picture for Co-Pt film plated at room temperature on top of Si(100) and Ti/Cu seed layer with direct current of $J = 20$ mA/cm^2.

Deposition of Co-Pt at higher temperature increases the mass transfer, reduces the grain size, and minimizes the surface cracking. Figure 10(b) shows the SEM (Scanning Electron Microscopy) structure of Co-Pt that is plated on top of the Si(100) and Ti/Cu seed layers

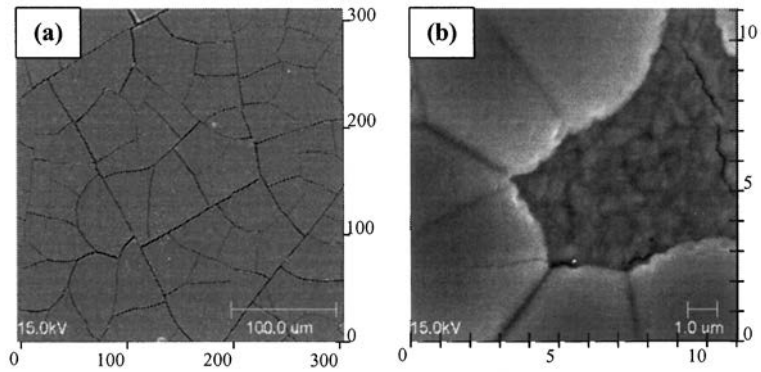

Fig. 9. The Co-Pt film deposited on top of Si(100) and Ti/Cu seed layer (dimensions are in μm). (a) J = 20 mA/cm^2 deposited at room temperature, 20°C ; (b) J = 25 mA/cm^2, deposited at temperature of 50°C.

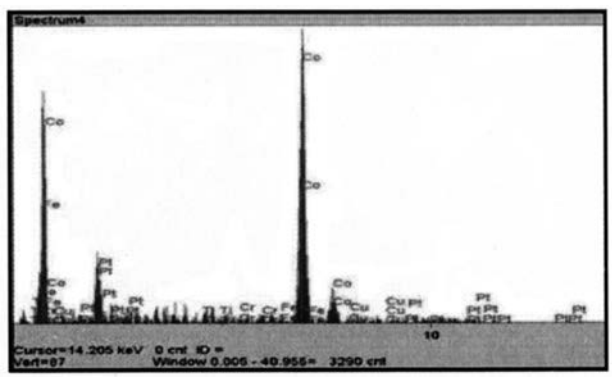

Fig. 10. Composition of the Co-Pt permanent magnet measured by EDX; the percentages of weight are: Co = 84.5%; Pt = 12.5%; Cu = 1.35%; and Fe = 0.79%.

with the direct current of J = 25 mA/cm^2 at the electrolyte temperature of 50°C. Figure 10(b) shows a 7000× magnification of the film. It shows that the grain can be divided into two main types according to the size: major grain size and minor grain size (D_h < 0.5 μm). Some minor cracking occurred in the minor grain size with a size of roughly 100 nm. The figure shows that the film consists of 70% major grain size; this indicates that the surface is not very smooth. Another approach to slightly improve the bubble production and increase the surface quality is to electroplate the Co-Pt magnet by pulsed current at J = 20–30 mA/cm^2, duty ratio = 40%, and bias = –10%. However, the deposition rate becomes very slow and it takes much longer to electroplate. Thus, direct current electroplating at J = 25–30 mA/cm^2 was used for fabricating the Co-Pt magnet with the deposition rate of 0.2–0.22 μm/min.

Figure 11 shows the composition of the deposited Co-Pt measured on a separate sample by EDX. The deposition was done on top of Si(100) and Ti/Cu seed layer with a direct current of J = 30 mA/cm^2 and an electrolyte temperature of 50°C with no magnetic stirring. It shows that the major contents are Co and Pt, with the weight composition of 84.5% and 12.5%. Other minor compositions are Cu and Fe. This is consistent with the reported literature,[67] where the Co-Pt composition is about 80 and 20% respectively. The experiment showed that with the addition of magnetic stirring, an increase in the Co composition to 90% and a decrease in the Pt composition to 7% were observed.

Ideally, we prefer to have a pure cobalt as the permanent magnet material due to it large coercivity (Ho) and magnetic saturation (Bs), however, pure cobalt is a "brittle" material, and it is almost impossible to electroplate without other impurities. The higher the cobalt content the higher the tensile stress which occurs during plating, which makes it extremely very hard to pattern. CoPt magnet has a large Ho and Bs at thin film thickness (t < 1 um).[67] The magnetic properties decrease with the thickness as the grain structure becomes more isotropic. In this microvalve we need to have thickness of more than 20 um. Although, we were successful with plating and patterning 25 um thick CoPt, the properties were changed but the CoMnNiP alloy did maintain its magnetic properties for thick electroplated films.

4.4 *CoNiMnP electroplating*

CoNiMnP is one of the alloys selected to fabricate the permanent magnet for the bistable microvalve. The recipe of the electrolyte is adapted from ref. 43 and modified for our purpose as in Table 5.

The electroplating process for the CoNiMnP is a little different than for CoPt. In order to improve the vertical anisotropy of the permanent magnet, CoNiMnP is plated inside a constant magnetic field. The electroplating bath is located in between ceramic magnets (Ferrimag 8A, Adams Magnetic Products, 3900 G). The produced constant magnetic field

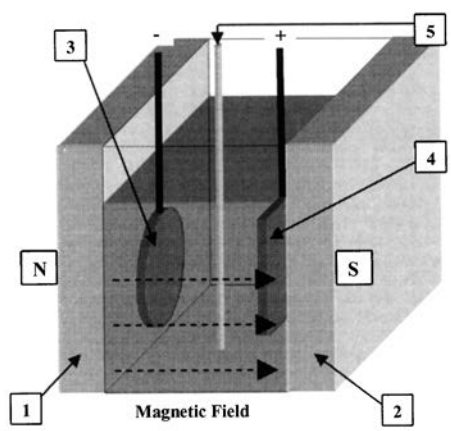

Fig. 11. Schematic illustration of electroplating setup for CoNiMnP; where: 1, 2 = ceramic magnets, 3 = 4 inch diameter silicon wafer, 4 = Anode, 4x4 inches Co plate, 5 = N_2 gas supply.

Table 5
Chemical composition of electroplating bath for CoNiMnP permanent magnet.

Chemical name	Chemical compound	gr/L
Cobalt chloride heptahydrate	$CoCl_2 . 6H_2O$	24
Nickel chloride hexahydrate	$NiCl_2 . 6H_2O$	24
Manganese sulfate monohydrate	$MnSO_4 . H_2O$	3.6
Sodium hypophosphite	$NH_2PO_2 - xH_2O$	4.6
Boric acid	H_3BO_3	22
Sodium lauryl sulfate	$CH_3(CH_2)_{11}OSO_3Na$	0.2
Saccharin		2
Sodium chloride	NaCl	22

between the ceramic magnets is measured by magnetometer and is about 800 G. In order to remove the gas bubbles produced on the electroplated CoNiMnP magnet and to ensure uniform concentration of solution inside the bath, nitrogen (N_2) gas is constantly supplied to the solution. Figure 12 below shows the schematic of CoNiMnP electroplating. Co foil is used as an anode to maintain the constant metal ion composition in the bath. The electroplating is performed with a pulsed current at J = 5–10 mA/cm^2, DR = 40%, and bias of –10 %. The electrolyte is maintained at room temperature with the pH level of 3–4.

5. Fabrication Results

5.1 *Bidirectional microactuator*

The fabrication of the bistable microvalve is far more difficult than that of the on/off valve. The addition of an electroplated permanent magnet integrated on the bottom of the centered soft magnetic membrane proves more difficult than might be first imagined. The fabrication needs extremely great patience. The surface roughness of the permanent magnet is not as suitable as soft magnetic material (NiFe). As mentioned before that the surface is mainly caused by the bubble generation during electroplating. The rough surface profile is patterned to the next electroplated layer, which is the soft magnetic membrane.

As mentioned, there were two different electroplated permanent magnet materials examined for the layer defined on the membrane of the microvalve to produce the bistable mechanism. These were CoPt and CoMnNiP permanent magnets. Unfortunately, the CoPt magnet did not provide a satisfactory bistable mechanism due to decrease in the magnetic properties. The wafer condition after the fabrication process as reported in ref. 64 and 65 is very unsatisfactory and makes it impossible to carry on the backside alignment and etch a hole through the back of the wafer. However, the integration of the CoMnNiP magnet on the soft magnetic membrane produces a bidirectional microactuator with a large membrane's displacement in both vertical directions. The experimental static and dynamic responses of the microactuator are reported in ref. 68.

The fabrication results of the bidirectional microactuator are shown in Figs. 12 and 13. It is shown that the membrane (label no. 5) is supported by two spring-designed legs (label no. 6) that are anchored to the circular support (label no. 4), the other leg is free. All legs

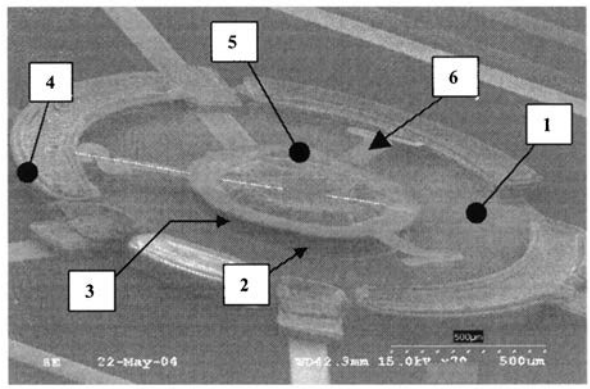

Fig. 12. SEM micrograph of bidirectional actuator with double-legs design; 1 = Orthonol base; 2 = microcoil; 3 = Co-Pt permanent magnet plated on the bottom of membrane; 4 = circular supports; 5 = Soft magnetic centered membrane; and 6 = membrane's supported legs.

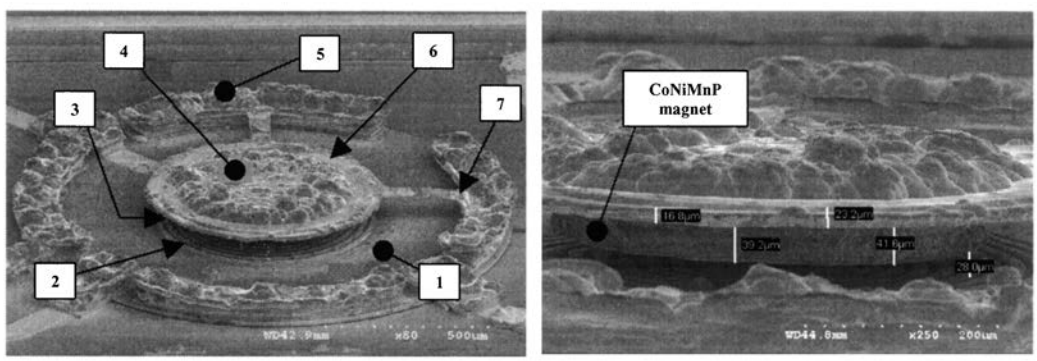

Fig. 13. SEM micrograph picture of the bistable microvalve, Where: 1 = Orthonol base; 2 = Au microcoil; 3 = CoMnNiP magnet; 4 = Membrane; 5 = Soft magnetic (Permalloy) centered membrane; and 6 = Membrane's supported legs.

are separated by a 120° angle. The distance between the center of the membrane and the top surface of the microcoil is about 70 µm. The measured dimensions of the bidirectional actuators are shown in Table 6.

5.2 *Bistable microvalve*

The integration of CoMnNiP magnet onto the membrane has been able to successfully create a bistable mechanism for the microvalve. The bistable and bidirectional tests for the membrane actuator in the medium of air are reported in ref. 65. The design, microfabrication, and liquid tests of the microvalve in the flow rate of water are reported in ref. 41. Figure 9 shows the SEM pictures of the bistable microvalve. It illustrates clearly the main

Table 6
Measured geometry of the bidirectional microactuator.

Overall diameter ($D_{overall}$)	1600	μm
Base thickness (t_{base})	10	μm
Gap/actuation displacement (g)	70	μm
Magnet thickness (t_M)	25	μm
Magnet diameter (D_M)	500	μm
Membrane diameter (D_1)	700	μm
Thickness of centered membrane (t_1)	21	μm
Thickness of legs (t_2)	2	μm
Legs width (w_2)	60	μm
Number of coils	12	
Width of the coil	14	μm
Thickness of the coils	8	μm

components of the microvalve. The microvalve has a membrane with 2 legs-design. The CoMnNiP magnet is electroplated on the soft magnetic membrane per the close up picture in Fig. 13.

Figure 12 shows a close up picture of the CoMnNiP magnet. It shows that the thickness of the magnet is about 39.2 μm. The thickness of the soft magnetic membrane is 23.2 μm. The gap distance between magnet and the bottom coil is measured to be 28 μm by SEM. The experimental measurement on the deflection of the membrane's center by Laser Doppler Vibrometer indicates, a maximum deflection of 30 μm.

6. Conclusions

A systematic approach to the design, modeling and fabrication of microvalves has benefits in generating prototypes with a greater chance of functional operation. The use of FEA is a key analysis tool that provides guidance for the choice of dimensions, and for evaluation of design alternatives, prior to committing to implementation of the fabrication processes. A number of different microvalves have been demonstrated and this illustrates some of the wealth of design space available. Future directions for study include optimization of the electomechanical drive for transient operation and a focus on minimization of power consumption. In our work the current applied to the coil was a constant for the duration of the actuator motion which results in an increasing force as the valve closes, however, it may be beneficial to change the current during the actuator motion to achieve, for example a constant force. Therefore, the use of open loop feedback control to optimize the dynamic performance could lower the power consumption and improve the lifetime of the valve. Additional areas for study include improved characterization techniques, improvements in fluid control, increased reliability and reduction of leakage. Finally, the properties of the electroplated magnetic materials have been taken from the literature, however, for more accurate modeling, measurements based upon the particular film

thicknesses used and processing conditions would be beneficial. This has not been an exhaustive survey and the details of processing implementation that allow integrated with CMOS electronics have not been addressed specifically, we leave these issues open for future research directions.

Acknowledgements

The authors would like to thank the Woodruff School of Engineering for financial support and from DARPA MTO-MPG office, Dr. Clark Nguyen Contract #F33615-01-2173. Many thanks to the staff at the Microelectronics Clean Room for their assistance in the fabrication of these devices and the members of the MEMS Group in the Woodruff School of Mechanical Engineering.

References

1 I. Chakraborty, W. C Tang, D. P. Bame and T. K. Tang: Sens. and Actuators, A **83** (2000) 188.
2 M. Esashi, S. Eoh, T. Matsuo and C. Choi: Transducers **87** (1987).
3 W. van der Wijngaart, J. Ask, P. Enokasson and G. Stemme: Sens. and Actuators, A **100** (2002) 264.
4 L. Yobas, M. A. Huff, F. J. Lisy and D. M. Durand: Journal of Microelectromechanical Systems **10** (2001) 187.
5 M. A. Huff, J. R. Gilbert and M. A. Schmidt: Technical Digest of the 7th International Conference on Solid-State Sensors and Actuators 1991.
6 K. Sato and M. Shikida: Journal of Micromechanics and Microengineering **4** (1994) 205.
7 C. Goll, W. Bacher, B. Bustgens, D. Maas, W. Menz and W. K. Schomburg: Journal of Micromechanics and Microengineering **6** (1996) 77.
8 S. Shoji: Electronics and Communications in Japan **82** (1999) 21.
9 S. Shoji and M. Esashi: Electronics and Communications in Japan **72** (1989) 52.
10 D. C. Roberts, H. Li, J. L. Steyn, O. Yaglioglu, S. M. Spearing, M. A. Schmidt and N. W. Hagood: Journal of Microelectromechanical Systems **12** (2003) 81.
11 S. Shoji, B. Van der Schoot, N. de Rooij and M. Esashi: Proceedings, Transducers "91 Int'l. Conf. Sol. State Sens. and Act., 1991.
12 M. Capanu, J. G. Boyd and P. J. Hesketh: Journal of Microelectromechanical Systems **9** (2000) 181.
13 R. L. Smith, R. W. Bower and S. D. Collins: Sens. and Actuators, A **24** (1990) 47.
14 K. Yanagisawa, H. Kuwano and A. Tago: Microsystem Technology **2** (1995) 22.
15 S. Bohm, G.J Burger, M.T. Korthorst and F. Roseboom: Sens. and Actuators, A **80** (2000) 77.
16 T. Lisec, H. J. Quenzer, M. Kreutzer, S. Horshelmann, B. Wagner and W. Benecke: Sensors and Materials **8** (1996) 13.
17 H. Jerman: Journal of Micromechanics and Microengineering **4** (1994) 210.
18 H. Jerman: Proceedings of Transducers '91, International Conference on Solid-State Sensors and Actuators, 1991.
19 P. W. Barth: Transducers '95, 1995.
20 C. A. Rich and K.D. Wise: J. Microelectromech. Systems **12** (2003) 201.
21 M. J. Zdeblick and J. B. Angell: Transducers '87, 1987.
22 M. J. Zdeblick, R. Anderson, J. Jankowski, B. Kline-Schoder, L. Christel, R. Miles and W. Eber: Proceedings of the Solid-State Sensor and Actuator Workshop, Hilton Head, SC, 1994.

23 M. Kohl, D. Dittmann, E. Quandt and B. Winzek: Sens. and Actuators, A **83** (2000) 214.
24 D. Johnson and C. A. Ray: (1994).
25 M. Kohl, K. D. Skrobanek, E. Quandt, P. Schlossmacher, A. Schussler and D. M. Allen: Journal de Physique IV, Colloque C8 (1995) 1167.
26 R. H. Liu, Q. Yu and D. J. Beebe: Journal of Microelectromechanical Systems **11** (2002) 45.
27 D. J. Beebe, J. S. Moore, J. M. Bauer, Q. Yu, R. H. Liu, C. Devadoss and B-H. Jo: Letter to Nature **404** (2000) 588.
28 D. T. Eddington and D. J. Beebe: Journal of Micromechanics and Microengineering **13** (2004) 586.
29 G. D. Gray and P. A. Kohl: Sens. and Actuators, A **119** (2005) 489.
30 G. D. Gray, E. M. Prophet, L. Zhu and P. A. Kohl: Sens. and Actuators, A **119** (2005) 502.
31 H. H. Yang, N. V. Myung, J. Yee, D.-Y. Park, B.-Y. Yob, M. Schwartz, K. Nobe and J. W. Judy: Sens. and Actuators A **97-98** (2002) 88.
32 J. W. Judy and R. S. Muller: Sens. and Actuators, A **53** (1996) 392.
33 E. Hill, W. A. F. Nor, J. K. Birtwistle and M. R. Parker: Sens. and Actuators, A **59** (2000) 30.
34 K. W. A. H. Oh, S. Bhansali and C. H. Ahn: Journal of Micromechanics and Microengineering **12** (2002) 187.
35 B. Bae, N. Kim, H. Kee, S-H. Kim, Y. Lee, S. Lee and K. Park: Journal of Microelectromechanical Systems **11** (2002) 344.
36 T. Ohori, S. Shoji, K. Miura and A. Yotsumoto: Sens. and Actuators, A **64** (1998) 57.
37 K. Hosokawa and R. Maeda: Journal of Microelectromechanics and Microengineering **10** (2000) 415.
38 J. Fahrenberg, W. Bier, D. Maas, W. Menz, R. Ruprecht and W.K. Schomburg: Journal of Micromechanics and Microengineering **5** (1995) 169.
39 C. M. Pemble and B. C. Towe: Sens. and Actuators, A **77** (1999) 145.
40 N. T. Nguyen, S. Schubert, S. Ricter and W. Dotzel: Sens. and Actuators, A **69** (1998) 85.
41 J. S. Bintoro and P. J. Hesketh: Journal of Micromechanics and Microengineering **15** (2005) 1157.
42 J. Sutanto, P. J. Hesketh and Y. H. Berthelot: Journal of Micromechanics and Microengineering **16** (2006) 266.
43 H. J. Cho and C. H. Ahn,: Journal of Microelectromechanical Systems **11** (2002) 78.
44 N. T. Nguyen and S. Wereley: Fundamentals and Applications of Microfluidics (Artech House, London, 2002).
45 K. W. Oh and Chong H. Ahn: Journal of Micromechanics and Microengineering **16** (2006) 13.
46 P. J. Hesketh, J. S. Bintoro and R. Luharuka: Microvalve for Fuel Cells and Miniature Gas Chromatographic System **13** (2003).
47 J. S. Bintoro and P. J. Hesketh: Journal of Micromechanics and Microengineering (2005) 1157.
48 M. Walters, V. Dhuler, R. Mahadevan, A. Cowen, R. Wood, E. Hill and I. Kao: Solid State Sensors and Actuators Workshop (Hilton Head, NC, 1998).
49 K. R. Williams, N. I. Maluf, E. N. Fuller, R. J. Barron, D. P. Jaeggi and B. P. van Drieënhuizen: 10th International Conference on Solid-State Sensors and Actuators (Transducers '99) (Sendai, Japan, 1999).
50 A. P. Papavasiliou, A. R. Pisano and D. Liepmann: Transducers (Munich, Germany, 2001).
51 S. J. A. F. Zimmermann, D. Liepmann and A. P. Pisano: Proceedings of the IEEE International Conference on Micro Electro Mechanical Systems (MEMS) (Maastricht, Netherlands, 2004).
52 S. Braun, S. Haasl, S. Sadoon, A. S. Ridgeway, W. Van Der Wijngaart and G. Stemme: Transducers (Seoul, South Korea, 2005).

53 A. K. Henning, J. S. Fitch, J. M. Harris, E. B. Dehan, B. A. Cozad, L. Christel, Y. Fathi, D. A. Hopkins, Jr., L. J. Lilly, W. McCulley, W. A. Weber and M. Zdeblick: IEEE Transactions on Components, Packaging, and Manufacturing Technology B **21** (1998) 329.
54 R. Luharuka and P. J. Hesketh: Sens. and Actuators, A (2006) (in press).
55 A. K. Henning: Transducers (2003).
56 A. K. Henning: MEMS/MOEMS Components and Their Applications (2004).
57 M. Capanu, J. G. I. Boyd and P. J. Hesketh: Journal of Microelectromechanical Systems **9** (2000) 181.
58 R. Luharuka and P. J. Hesketh: ASME International Mechanical Engineering Congress and Exposition (Orlando, Fl, 2005).
59 Z. Nami, C. H. Ahn and M. G. Allen: Journal of Micromechanics and Microengineering **6** (1996) 337.
60 D. Bosch, B. Heimhofer, G. Muck, H. Seidel, U. Thumser and W. Welser: Sens. and Actuators, A **37-38** (1993) 684.
61 R. C. O' Handley: Modern Magnetic Materials: Principles and Applications, 1st ed. (John Wiley and Sons, 2000).
62 J. S. Bintoro: Ph.D. dissertation in Mechanical Engineering. (Georgia Institute of Technology, Atlanta, 2004).
63 J. Donéa: Finite element analysis of transient dynamic fluid-structure interaction, 1st ed. (Applied Science Publishers, London, 1980).
64 J. S. Bintoro, P. J. Hesketh and Y. H. Berthelot: Microelectronics Journal **36** (2005) 667.
65 J. S. Bintoro, A. D. Papania, Y. H. Berthelot and P. J. Hesketh: Journal of Micromechanics and Microengineering **15** (2005) 1378.
66 J. Y. Park and M. G. Allen: IEEE Transactions on Electronics Packaging Manufacturing **23** (2000) 48.
67 I. Zana and G. Zangari: Electrochemical and Solid-State Letters **6** (2003) 153.
68 J. Bintoro and A. D. Papania, Y. H. Berthelot and P. J. Hesketh: Microelectron. Eng. **82** (2005) 12.